The American Journal of Pathology, Vol. 180, No. 3, March 2012
Copyright © 2012 American Society for Investigative Pathology.
Published by Elsevier Inc. All rights reserved.
DOI: 10.1016/j.ajpath.2011.11.010

Short Communication

Inflammation-Induced Lymph Node Lymphangiogenesis Is Reversible

Viviane Mumprecht, Filip Roudnicky, and Michael Detmar

From the Institute of Pharmaceutical Sciences, Swiss Federal Institute of Technology, ETH Zurich, Zurich, Switzerland

The extent of lymph node metastasis is a prognostic indicator of disease progression in many malignancies. Current noninvasive imaging technologies for the clinical assessment of lymph node metastases are based on the detection of cancer cells and commonly suffer from a lack of sensitivity. Recent evidence has indicated that the expansion of lymphatic networks (ie, lymphangiogenesis) within tumor-draining lymph nodes might be the earliest sign of metastasis. Therefore, we recently developed a noninvasive imaging method to visualize lymph node lymphangiogenesis in mice using radiolabeled antibodies against the lymphatic vessel endothelial hyaluronan receptor-1 (LYVE-1) as well as positron emission tomography (PET). This technique, termed anti-LYVE-1 immuno-PET, was found to be very sensitive in the detection of metastasis to the lymph nodes. However, lymphatic vessel expansion to the lymph nodes can also be induced by inflammation, and it is currently unclear whether such vessel expansion is reversed once inflammation has resolved. Detection of residual inflammation-induced lymph node lymphangiogenesis, thus, might hamper the identification of metastasized lymph nodes. In this study, we therefore used a well-established mouse model of inflammation in the skin to investigate whether lymphatic vessels in the lymph nodes regress on resolution of inflammation. Our data reveal that the lymphatic network indeed regresses on the resolution of inflammation and that we can image this process by anti-LYVE-1 immuno-PET. ***(Am J Pathol 2012, 180:874–879; DOI: 10.1016/j.ajpath.2011.11.010)***

Metastasis to the lymph nodes is a prognostic indicator for disease progression in many malignancies. Current noninvasive imaging technologies to assess lymph node metastases in clinics are based on the detection of cancer cells. However, these methods have limited sensitivities because a large number of tumor cells are required for reliable detection.[1] Recently, our group, along with others, found that cancers can induce the expansion of the lymphatic vasculature (lymphangiogenesis) in draining lymph nodes in experimental models and in cancer patients.[2–7] Importantly, lymph node lymphangiogenesis occurs very early during the process of tumor metastasis, and it is associated with the spread of cancer cells to lymph nodes and organs.[4,7] Because lymphatic vessel expansion is already induced at the beginning of the metastatic process, we have previously suggested that it might serve as an early indicator for cancer metastasis to the lymph nodes.[8] We have, therefore, recently developed a method termed anti-lymphatic vessel endothelial hyaluronan receptor-1 (LYVE-1) immuno-positron emission tomography (PET) to image lymph node lymphangiogenesis noninvasively *in vivo*.[8] This technique is based on the intravenous injection of a radioactively-labeled antibody against LYVE-1, which is almost exclusively expressed on the lymphatic vessels.[9,10] Subsequently, the increased accumulation of injected ^{124}I-anti-LYVE-1 antibody in the lymphangiogenic lymph nodes is imaged by PET. Anti-LYVE-1 immuno-PET detected lymphatic vessel expansion in metastasized lymph nodes that were not detected by ^{18}F-fluorodeoxyglucose-PET that is currently applied in clinics.[8] These data suggested that imaging of lymph node lymphangiogenesis might be a new strategy for the early detection of cancer metastasis.

Studies in experimental models, however, showed that lymphatic network expansion in the lymph nodes can also be induced by inflammation, and we have demonstrated that this process is detected by anti-LYVE-1 immuno-PET as well.[8,11–13] Currently, it is unclear whether

Supported in part by the National Institutes of Health (grant CA69184), Swiss National Science Foundation (grant 3100A0-108207), Cancer League Zurich, Oncosuisse and Advanced European Research Council grant LYVICAM (M.D.).

Accepted for publication November 14, 2011.

Address reprint requests to Michael Detmar, M.D., Institute of Pharmaceutical Sciences, Swiss Federal Institute of Technology, ETH Zurich, Wolfgang-Pauli-Str. 10, HCI H303, CH-8093 Zurich, Switzerland. E-mail: michael.detmar@pharma.ethz.ch.

lymphatic vessels regress after resolution of inflammation. In a model of bacterial-induced airway inflammation, lymphatic vessels in the trachea persisted after the inflammation had subsided.[14] It is thus conceivable that detection of persistent lymph node lymphangiogenesis, after previously regressed inflammatory processes in the draining area of the sentinel lymph node, in cancer patients might hamper the reliable identification of metastatic lymph nodes. In this study, therefore, we aimed to investigate whether lymphatic vessel expansion in the lymph nodes is reversible, using an established model of inflammation in the skin.[12] After induction of a delayed-type hypersensitivity reaction in the ear skin, these mice develop skin inflammation that is associated with pronounced expansion of the lymphatic network within the draining superficial parotid lymph nodes (also termed auricular lymph nodes). After discontinuing the inflammatory stimulus, the inflammation in the ear skin resolves.

Our results reveal that the expansion of the lymphatic network in the lymph nodes is indeed reversed after resolution of inflammation and that this process can be imaged by anti-LYVE-1 immuno-PET.

Materials and Methods

Inflammation-Induced Lymph Node Lymphangiogenesis

Female FVB mice (Charles River Laboratories, Wilmington, MA) were assigned into three treatment groups ($n = 3$ per group): i) mice in which delayed-type hypersensitivity (DTH) reactions were induced in the ear skin (inflammation group); ii) mice in which DTH responses were induced as in the inflamed group, and in which the inflammation was subsequently allowed to regress (regression group); and iii) untreated control mice (control group) (Figure 1A).

DTH reactions were induced in the ear skins as described.[12] Briefly, the mice were sensitized by topical application of 2% of the allergen oxazolone (4-ethoxymethylene-2 phenyl-2-oxazoline-5-one; Sigma, St. Louis, MO) in acetone:olive oil (4:1 by volume) to their shaved abdomen (50 μL) and to the skin of each paw (5 μL each). Five days after sensitization (study day zero) and from then on every other day until study day 9, 10 μL of a 1% oxazolone solution was applied topically to each side of the ears to induce inflammation in the ear skin and lymphatic vessel expansion in the ear draining lymph nodes.[12] Mice of the inflamed group were then injected with ^{124}I-anti-LYVE-1 antibody and imaged by PET as described as follows. In contrast, in the regression group, oxazolone treatment was stopped after study day 9, and the mice were kept for an additional 3 months, to allow the inflammation in the ear skin to regress, and were then subjected to anti-LYVE-1 immuno-PET. Ear thickness was measured before the oxazolone challenge and was repeatedly measured after the challenge using calipers, which were used to read-out inflammation. At the time of PET imaging, all mice were in between 22- and 24-weeks-old.

Before the PET experiments, normal uptake of radiolabeled iodine by the thyroid glands and by iodine symporters in the intestine was blocked by administration of potassium iodide in the drinking water starting 4 days before injection of the radioactively labeled antibody, and by oral administration of sodium perchlorate 1 hour before antibody injection. All animal experiments were approved by the cantonal veterinarian office Zurich (Kantonales Veterinäramt Zürich).

Radioiodination and PET Imaging

Radioiodination of anti-LYVE-1 antibody was performed as described.[8] Briefly, three batches of 180 μg anti-LYVE-1 antibody (clone *223322*, R&D Systems, Minneapolis, MN) were each labeled with 74 MBq Na^{124}I (IBA Molecular, Louvain-La-Neuve, Belgium) by the chloramide T method. Then, the ^{124}I-anti-LYVE-1 antibody was purified with PD-10 columns (GE Healthcare, Chalfont St. Giles, UK). Subsequently, 38 μg of ^{124}I-anti-LYVE-1 antibody (11.1–12.4 MBq) were injected intravenously into the tail veins of the mice of the three treatment groups. Within 14 to 25 hours after antibody injection, the mice were scanned using a GE Vista/CT camera (GE Healthcare) as described.[15] For *in vivo* PET scanning, mice were anesthetized with isofluorane (Abbott Laboratories, Abbott Park, IL) in an air/oxygen mixture and monitored during PET scanning, as described.[16] Whole-body PET data were acquired in two bed positions (30 minutes acquisition time per position) and were reconstructed in a single time frame, with pixel sizes of 0.3875 mm and 0.775 mm in the transverse and axial directions, respectively. After scanning, the mice were sacrificed and the radioactivity in the superficial parotid lymph nodes was measured using a gamma counter (1480 Wizard Automatic Gamma Counter, Perkin Elmer, Waltham, MA). Data were corrected for the body weight of the mice and variations of the injected dose. PET sections were displayed with a fixed gray scale for comparison between different mice.

Microradiography and Immunofluorescence Analysis

After the PET experiments, the animals were sacrificed and the superficial parotid lymph nodes were frozen in optimal cutting temperature (OCT) compound (Sakura Finetec, Zoeterwoude, Netherlands). The lymph nodes were cut in 7 μm sections and fixed with 4% paraformaldehyde in PBS. Air-dried sections were coated with Kodak autoradiography emulsion type NTB (Carestream Health, Inc., Rochester, NY), and developed according to the manufacturer's instructions after 2 weeks exposure time. Alternatively, sections were fixed with 4% paraformaldehyde in PBS, incubated with an Alexa Fluor (AF) 594 conjugated donkey anti-rat IgG antibody (Invitrogen, Carlsbad, CA), and co-stained with a rabbit anti-mouse LYVE-1 antibody (Angiobio, Del Mar, CA) detected by an AF488 donkey anti-rabbit IgG antibody (Invitrogen). Sections were analyzed with an AxioScop2 MOT plus microscope (Zeiss, Oberkochen, Germany) and images were captured with an AxioCam MRc camera (Zeiss) using the Axio-Vision 4.7 software.

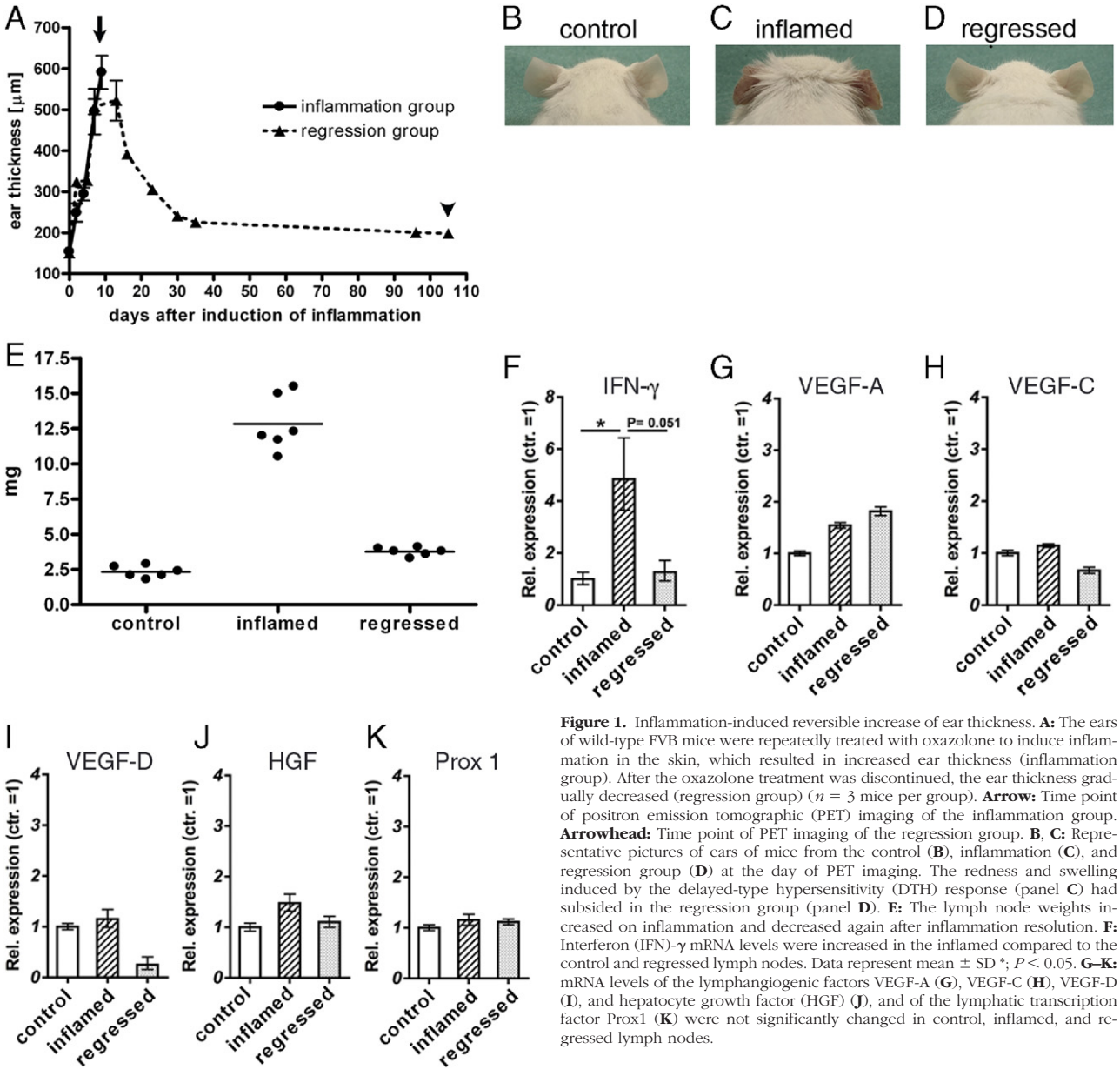

Figure 1. Inflammation-induced reversible increase of ear thickness. **A:** The ears of wild-type FVB mice were repeatedly treated with oxazolone to induce inflammation in the skin, which resulted in increased ear thickness (inflammation group). After the oxazolone treatment was discontinued, the ear thickness gradually decreased (regression group) ($n = 3$ mice per group). **Arrow:** Time point of positron emission tomographic (PET) imaging of the inflammation group. **Arrowhead:** Time point of PET imaging of the regression group. **B**, **C:** Representative pictures of ears of mice from the control (**B**), inflammation (**C**), and regression group (**D**) at the day of PET imaging. The redness and swelling induced by the delayed-type hypersensitivity (DTH) response (panel **C**) had subsided in the regression group (panel **D**). **E:** The lymph node weights increased on inflammation and decreased again after inflammation resolution. **F:** Interferon (IFN)-γ mRNA levels were increased in the inflamed compared to the control and regressed lymph nodes. Data represent mean ± SD *; $P < 0.05$. **G–K:** mRNA levels of the lymphangiogenic factors VEGF-A (**G**), VEGF-C (**H**), VEGF-D (**I**), and hepatocyte growth factor (HGF) (**J**), and of the lymphatic transcription factor Prox1 (**K**) were not significantly changed in control, inflamed, and regressed lymph nodes.

RNA Isolation and Quantitative Real-Time PCR

Total cellular RNA was isolated from frozen superficial parotid lymph nodes using a TissueLyser, stainless steel beads, and the RNeasy Plus Micro kit (all from QIAGEN, Hilden, Germany). RNA (1.2 μg) was used to synthesize cDNA using the High-Capacity cDNA Reverse Transcription kit (Applied Biosystems, Foster City, CA). The expression of murine interferon (IFN)-γ, hepatocyte growth factor, Prox1, vascular endothelial growth factor (VEGF)-A, -C, and -D was investigated by TaqMan real-time PCR using the AB 7900 HT Fast Real-Time PCR System (Applied Biosystems) and quantified using the $2^{-\Delta\Delta C_T}$ method.[17] The probes and primers for IFN-γ (Mm01168134_m1), hepatocyte growth factor (Mm01135193_m1), Prox1 (Mm00435971_m1), VEGF-A (Mm00443258_m1), VEGF-C (Mm01202432_m1), and VEGF-D (Mm00438965_m1) were predesigned. Each reaction was multiplexed with β-actin (4352341E; all from Applied Biosystems) as a reference gene and all data were normalized based on the expression levels of β-actin ($n = 3$ per group).

Results

Induction and Resolution of Skin Inflammation

To investigate whether resolution of inflammation leads to the regression of the expanded lymphatic vasculature in the lymph nodes, we used an established mouse model of ear skin inflammation.[12] After topical application of the contact sensitizer oxazolone, the mice developed inflammation in the ear skin that was associated with inflammation and prominent lymphangiogenesis in the ear draining superficial

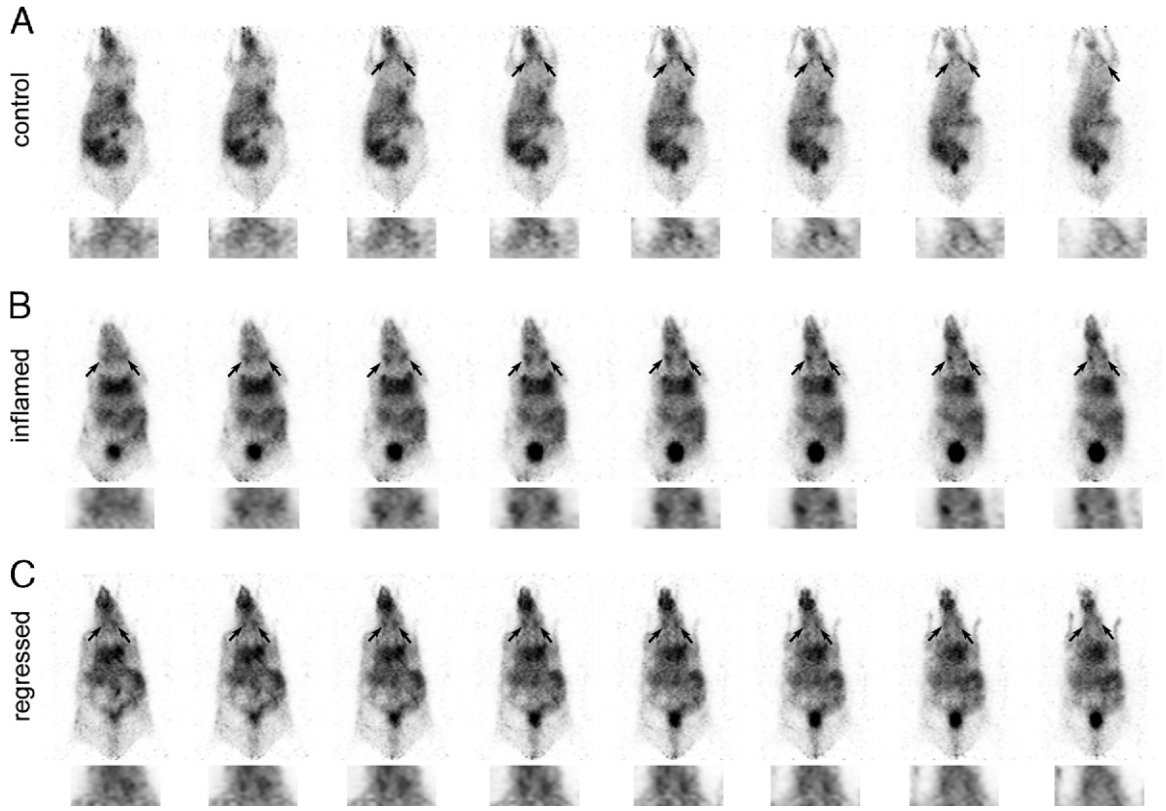

Figure 2. In vivo positron emission tomographic (PET) imaging of the lymphatic vessel regression in superficial parotid lymph nodes using ^{124}I-anti-lymphatic vessel endothelial hyaluronan receptor-1 (LYVE-1) antibody. **A–C:** Normalized serial PET sections of mice from the control (**A**), inflammation (**B**), and regression groups (**C**) ($n = 3$ per group) with higher magnifications of the cervical regions below. The accumulation of ^{124}I-anti-LYVE-1 antibody in the superficial parotid lymph nodes (**arrows**) was stronger in inflammation than in the control group. Regression of inflammation subsequently resulted in reduced accumulation of ^{124}I-anti-LYVE-1 antibody in the lymph nodes.

parotid lymph nodes. We have measured the ear thickness before and after DTH-response induction as a readout of inflammation. Oxazolone treatment induced reddening and inflammation of the ear skin and increased the ear thickness from 148 ± 2 μm before inflammation to 520 ± 8 μm at study day nine (Figure 1, A–C). After discontinuation of the oxazolone treatment, the ear erythema gradually disappeared, and after 3 months the ear thickness was reduced to 198 ± 10 μm, which indicated that the inflammation had largely resolved. In addition to inflammation in the ear skin, the DTH response provoked a 5.6-fold increase in lymph node weights that was almost reversed in the regressed group (Figure 1E). Accordingly, the mRNA expression levels of the inflammatory cytokine IFN-γ were significantly increased in inflamed lymph nodes, and were back to normal levels in the regression group (Figure 1F). No major changes in mRNA expression were observed for the lymphangiogenic factors VEGF-A, VEGF-C, VEGF-D, and hepatocyte growth factor, or for the lymphatic transcription factor Prox1 (Figure 1, G–K).

In Vivo *PET Imaging Reveals Lymphatic Vessel Expansion and Regression in Draining Lymph Nodes*

Next, we visualized the ear-draining superficial parotid lymph nodes by anti-LYVE-1 immuno-PET and assessed whether the radioactive signals at these sites decreased after resolution of the inflammation. Thus, we radiolabeled the anti-LYVE-1 antibody with the positron emitter ^{124}I and administered it intravenously into mice of the control, inflammation, and the regression group. *In vivo* PET imaging was performed 14 to 25 hours after antibody injection. Normalized serial sections of the mice revealed much stronger radioactive signals in the superficial parotid lymph nodes of the inflammation group compared to the control group (Figure 2, A and B), indicating that the lymphatic vasculature had indeed expanded in lymph nodes draining inflamed skin. To validate this finding, we sacrificed the mice and measured the radioactivity in the isolated superficial parotid lymph nodes with a gamma counter. Inflamed lymph nodes had accumulated 7.3-fold more ^{124}I-anti-LYVE-1 antibody ($6.5 \times 10^5 \pm 0.6 \times 10^5$ cpm) than control lymph nodes ($8.9 \times 10^4 \pm 3.1 \times 10^4$ cpm) (Figure 3). The radioactive signals in the lymph nodes of ^{124}I-anti-LYVE-1 antibody injected mice were specific since ^{124}I-labeled control IgG does not accumulate in the lymphatic vessels, as we have previously shown.[8]

Next, we investigated normalized sections of the mice of the regression group, in which inflammation was allowed to resolve. Importantly, the signal in these mice was strongly reduced compared to the inflammation group (Figure 2, B and C). The clear difference in antibody accumulation was confirmed by measuring the iso-

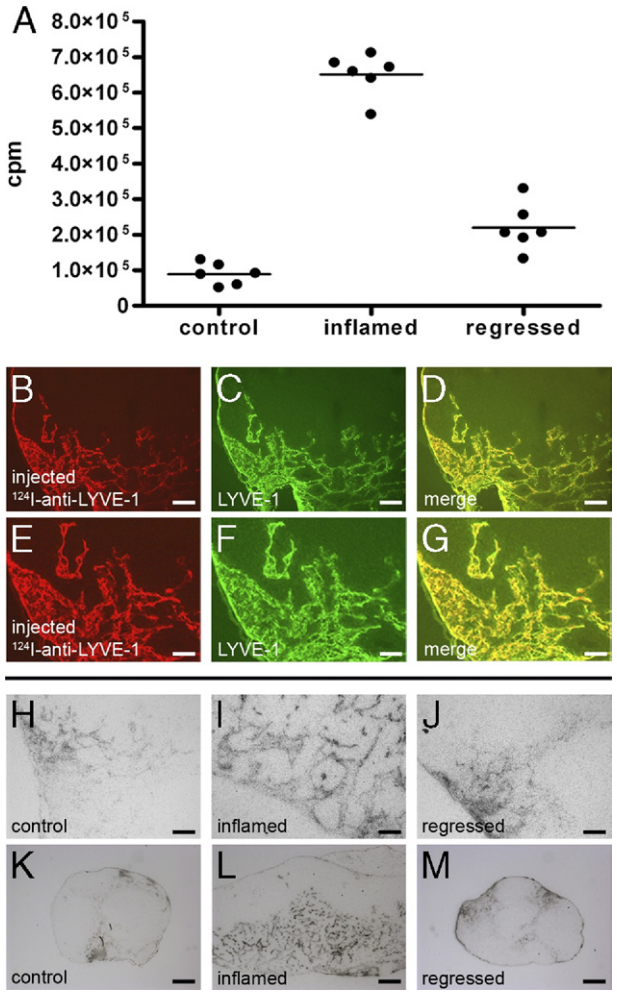

Figure 3. Reversible expansion of the lymphatic network in the lymph nodes on inflammation. **A:** Radioactivity in the superficial parotid lymph nodes of the mice was measured subsequent to positron emission tomographic (PET) imaging. Inflammation in the ear skin resulted in increased antibody accumulation in the draining lymph nodes. On inflammation resolution, antibody accumulation was decreased again ($n = 3$ mice per group; cpm = counts of gamma quantum stemming from ^{124}I decays per minute). **B–D:** Immunofluorescence analysis of a representative tissue section from an inflamed superficial parotid lymph node. The injected ^{124}I-anti-LYVE-1 antibody (**B**) completely co-localized with LYVE-1 stained lymphatic vessels (**C**); (merge, **D**). Scale bars: 100 μm. **E–G:** Higher magnifications of panels **B–D**, respectively. Scale bars: 50 μm. **H–J:** Microradiographs of tissue sections of control (**H**), inflammation (**I**), and regression groups (**J**) mice following immuno-PET imaging reveal increased accumulation of the injected ^{124}I-anti-LYVE-1 antibody (black signal) in the inflamed compared to the regressed or the control lymph node. Scale bars = 100 μm. **K–M:** Low magnifications of micrographs of control, inflamed, and regressed lymph nodes, respectively. Scale bars: 200 μm.

lated lymph nodes, which revealed a 66% decrease in antibody accumulation ($2.1 \times 10^5 \pm 0.7 \times 10^5$ cpm) compared to the inflamed lymph nodes (Figure 3A).

Inflammation Resolution Leads to Lymphatic Vessel Regression

In an additional step, we determined the location of the injected ^{124}I-anti-LYVE-1 antibody in the superficial parotid lymph nodes of the different groups after PET imaging. We detected the injected ^{124}I-anti-LYVE-1 antibody by a fluorescently labeled anti-rat IgG antibody on lymph node sections (Figure 3, B and E). Importantly, the localization of the injected anti-LYVE-1 antibody overlapped completely with the localization of LYVE-1 when detected by external co-staining with a rabbit antibody to LYVE-1 (Figure 3, C, D, F, and G), which indicates that all lymphatic structures in the lymph nodes were reached by the antibody.

Microradiography of superficial parotid lymph node sections from the control, inflammation, and regression groups revealed equally strong signals of the injected ^{124}I-anti-LYVE-1 antibody on the lymphatic vessels (Figure 3, H-M), indicating that the lymphatic vessels of the three groups were equally accessible for the antibody. However, microradiographies revealed a much larger amount of lymphatic vessels in the inflamed than in the control lymph nodes (Figure 3, H, I, K, and L), which confirms the increased radiolabeled antibody accumulation observed in PET imaging and in the excised superficial parotid lymph nodes. Importantly, the amount of lymphatic vessels decreased on inflammation regression (Figure 3, J and M).

Taken together, these data indicate that the lymphatic vasculature in the lymph nodes (that has expanded on inflammation) regresses after resolution of inflammation and we can image this process by anti-LYVE-1 immuno-PET.

Discussion

In this study we have shown that inflammation-induced lymphatic vessel expansion in lymph nodes is reversible and we can image this process by anti-LYVE-1 immuno-PET.

We have previously found that solid tumors induce the expansion of the lymphatic vasculature in the draining lymph nodes of experimental mouse models, along with others,[2–5,18] and in melanoma and breast cancer patients.[6,7] This process starts at the beginning of cancer metastasis and therefore its noninvasive visualization might represent a novel approach for cancer metastasis detection.[8] The detection of inflammation-induced lymph node lymphangiogenesis might complicate the identification of metastasized lymph nodes. However, the data presented here indicate that inflammation-induced lymphatic vessel expansion in the lymph nodes is reversible. Thus, resolved inflammations will not be detected (or will only weakly be detected) by noninvasive lymphatic vessel imaging. Because inflammation and tumors rarely co-exist at the same location and drain into the same lymph nodes, detection of lymph node lymphangiogenesis might therefore likely indicate cancer metastasis to these sites and not a previous occurrence of inflammation in the area that drains to the sentinel lymph node.

Currently, there are few data on the possible molecular mechanisms that regulate lymphatic vessel regression. A recent report indicated that IFN-γ might mediate reduction of lymphatic vessels in a model of bacterial pathogen-induced lymph node lymphangiogenesis.[18] However, in our study we found increased IFN-γ transcript levels in the inflamed compared to the control and the regressed lymph nodes, therefore largely ruling out a major role of

IFN-γ in mediating lymphatic vessel regression. Previously, lymphangiogenesis in the lymph nodes has been reported to be induced by vascular endothelial growth factors secreted by macrophages and B-cells.[11,13] Our expression studies, however, showed no major changes in the mRNA expression levels of the lymphangiogenic factors hepatocyte growth factor and VEGF-A, -C, and -D in the affected lymph nodes. We have previously found that lymph node lymphangiogenesis in the inflammation model used in this study was induced by VEGF-A that drained from the inflamed ear skin.[12] Thus, reduced skin inflammation in the regressed group likely resulted in diminished amounts of VEGF protein transported via lymphatic vessels to the draining lymph nodes. Interestingly, lymphatic vessel regression only started once the inflammation had substantially resolved. One month after discontinuing the inflammatory stimulus, we have not found a decrease in ^{124}I-anti-LYVE-1 antibody accumulation in the lymph nodes compared to the inflamed mice (data not shown).

In a model of bacterial-induced airway inflammation lymphatic vessels in the trachea only partially regressed after the inflammation had subsided. However, in this model, lymphatic vessels were investigated in the peripheral tissue itself, whereas we analyzed the lymphatic vessels in the lymph nodes, not in the peripheral (inflamed) tissue. Thus, there may be model-specific and site-specific differences of the lymphatic vessel response to inflammation regression.

In conclusion, our data indicate that inflammation does not leave a permanent lymphatic vessel "scar" in the lymph nodes, and they also suggest that imaging of lymphatic vessel expansion in lymph nodes might be a promising strategy for the early detection of cancer metastasis.

Acknowledgments

We are grateful to Claudia Keller and Petra Wirth for technical support.

References

1. Jaffer FA, Weissleder R: Molecular imaging in the clinical arena. Jama 2005, 293:855–862
2. Hirakawa S, Kodama S, Kunstfeld R, Kajiya K, Brown LF, Detmar M: VEGF-A induces tumor and sentinel lymph node lymphangiogenesis and promotes lymphatic metastasis. J Exp Med 2005, 201:1089–1099
3. Qian CN, Berghuis B, Tsarfaty G, Bruch M, Kort EJ, Ditlev J, Tsarfaty I, Hudson E, Jackson DG, Petillo D, Chen J, Resau JH, Teh BT: Preparing the "soil": the primary tumor induces vasculature reorganization in the sentinel lymph node before the arrival of metastatic cancer cells. Cancer Res 2006, 66:10365–10376
4. Hirakawa S, Brown LF, Kodama S, Paavonen K, Alitalo K, Detmar M: VEGF-C-induced lymphangiogenesis in sentinel lymph nodes promotes tumor metastasis to distant sites. Blood 2007, 109:1010–1017
5. Harrell MI, Iritani BM, Ruddell A: Tumor-induced sentinel lymph node lymphangiogenesis and increased lymph flow precede melanoma metastasis. Am J Pathol 2007, 170:774–786
6. Dadras SS, Lange-Asschenfeldt B, Velasco P, Nguyen L, Vora A, Muzikansky A, Jahnke K, Hauschild A, Hirakawa S, Mihm MC, Detmar M: Tumor lymphangiogenesis predicts melanoma metastasis to sentinel lymph nodes. Mod Pathol 2005, 18:1232–1242
7. Van den Eynden GG, Vandenberghe MK, van Dam PJ, Colpaert CG, van Dam P, Dirix LY, Vermeulen PB, Van Marck EA: Increased sentinel lymph node lymphangiogenesis is associated with nonsentinel axillary lymph node involvement in breast cancer patients with a positive sentinel node. Clin Cancer Res 2007, 13:5391–5397
8. Mumprecht V, Honer M, Vigl B, Proulx ST, Trachsel E, Kaspar M, Banziger-Tobler NE, Schibli R, Neri D, Detmar M: In vivo imaging of inflammation- and tumor-induced lymph node lymphangiogenesis by immuno-positron emission tomography. Cancer Res 2010, 70:8842–8851
9. Banerji S, Ni J, Wang SX, Clasper S, Su J, Tammi R, Jones M, Jackson DG: LYVE-1, a new homologue of the CD44 glycoprotein, is a lymph-specific receptor for hyaluronan. J Cell Biol 1999, 144:789–801
10. Prevo R, Banerji S, Ferguson DJ, Clasper S, Jackson DG: Mouse LYVE-1 is an endocytic receptor for hyaluronan in lymphatic endothelium. J Biol Chem 2001, 276:19420–19430
11. Angeli V, Ginhoux F, Llodra J, Quemeneur L, Frenette PS, Skobe M, Jessberger R, Merad M, Randolph GJ: B cell-driven lymphangiogenesis in inflamed lymph nodes enhances dendritic cell mobilization. Immunity 2006, 24:203–215
12. Halin C, Tobler NE, Vigl B, Brown LF, Detmar M: VEGF-A produced by chronically inflamed tissue induces lymphangiogenesis in draining lymph nodes. Blood 2007, 110:3158–3167
13. Kataru RP, Jung K, Jang C, Yang H, Schwendener RA, Baik JE, Han SH, Alitalo K, Koh GY: Critical role of CD11b+ macrophages and VEGF in inflammatory lymphangiogenesis, antigen clearance, and inflammation resolution. Blood 2009, 113:5650–5659
14. Baluk P, Tammela T, Ator E, Lyubynska N, Achen MG, Hicklin DJ, Jeltsch M, Petrova TV, Pytowski B, Stacker SA, Yla-Herttuala S, Jackson DG, Alitalo K, McDonald DM: Pathogenesis of persistent lymphatic vessel hyperplasia in chronic airway inflammation. J Clin Invest 2005, 115:247–257
15. Wang Y, Seidel J, Tsui BM, Vaquero JJ, Pomper MG: Performance evaluation of the GE healthcare eXplore VISTA dual-ring small-animal PET scanner. J Nucl Med 2006, 47:1891–1900
16. Honer M, Bruhlmeier M, Missimer J, Schubiger AP, Ametamey SM: Dynamic imaging of striatal D2 receptors in mice using quad-HIDAC PET. J Nucl Med 2004, 45:464–470
17. Schmittgen TD, Livak KJ: Analyzing real-time PCR data by the comparative C(T) method. Nat Protoc 2008, 3:1101–1108
18. Kataru RP, Kim H, Jang C, Choi DK, Koh BI, Kim M, Gollamudi S, Kim YK, Lee SH, Koh GY: T lymphocytes negatively regulate lymph node lymphatic vessel formation. Immunity 2011, 34:96–107